

# Application of electrical resistivity imaging to the development of a geologic model for a proposed Edmonton landfill site

Lindsay N. Meads, Laurence R. Bentley, and Carl A. Mendoza

**Abstract:** Electrical resistivity imaging (ERI) was used to further characterize the geologic setting at the proposed Aurum solid-waste landfill site near Edmonton, Alberta. Two bedrock channel aquifers, the east and south channels, exist in or near the site. Previous studies at the proposed site used borehole and pumping test data to determine that the two aquifers are separate and hydraulically disconnected by a sheet of ice thrust bedrock. The three objectives of the ERI were to resolve the sand channels and terrace sands, resolve the top of the thrust bedrock, and resolve the sand channels beneath the thrust bedrock. The ERI survey, in combination with the borehole data, presented a more detailed representation of the site's complex geology than borehole data alone. The south channel has a long and even bottom, steeply sloping sides, and two levels. The thrust bedrock occurs as irregular massive blocks throughout the site, and the aquifers are hydraulically confined by the glacial till. The bedrock surface is highly variable where it has been modified by glacial ice thrusting and relatively uniform elsewhere. Electrical resistivity imaging was found to be useful for the prompt and accurate development of a geologic model for the proposed Aurum landfill site.

*Key words:* electrical resistivity imaging, thrust bedrock, site characterization.

**Résumé :** On a utilisé l'imagerie par résistivité électrique (IRE) pour caractériser davantage le cadre géologique sur le site proposé de l'enfouissement sanitaire de résidus solides d'Aurum près d'Edmonton, Alberta. Il existe sur ou près du site deux canaux d'aquifères dans le socle rocheux, les canaux de l'est et du sud. Dans les études antérieures sur le site proposé, on a utilisé des données de forages et d'essais de pompage pour déterminer que les deux aquifères sont séparés et isolé l'un de l'autre du point de vue hydraulique par une couche de lit rocheux charriée par la glace. Les trois objectifs d'imagerie ont été de définir les canaux et les terrasses de sable, définir le dessus du lit de roc charrié, et définir les canaux de sable sous le lit rocheux charrié. Le relevé à l'IRE, combiné avec les données des forages, ont fourni une représentation de la géologie complexe du site plus détaillée que les données des forages seules. Le canal sud a un fond plat et long, des côtés en pentes abruptes, et deux niveaux. Le lit rocheux se présente sous la forme de blocs massifs irréguliers sur l'ensemble du site et les aquifères sont confinés du point de vue hydraulique par le till glaciaire. La surface du lit rocheux est extrêmement variable là où il a été modifié par le charriage des glaciers, et relativement uniforme ailleurs. On a trouvé que la technique d'IRE était utile pour le développement prompt et précis d'un modèle géologique pour le site d'enfouissement proposé d'Aurum.

*Mots clés :* imagerie par résistivité électrique, lit rocheux charrié, caractérisation de site.

[Traduit par la Rédaction]

## Introduction

### Location and background

The Aurum site was a proposed city of Edmonton waste management centre. The proposed solid-waste landfill site is located in Section 22, Township 53, Range 23, west of the 4th Meridian and lies 0.5 km south of the North Saskatche-

wan River (Andriashek et al. 1993). The study area is approximately 1.8 km by 1.8 km and is bounded by 137 Avenue N.E. to the north and 33 Street N.E. to the east (Fig. 1). Stanley Associates Engineering Ltd. conducted three detailed hydrogeologic investigations of the site from 1987 to 1990 (Stanley Associates Engineering Ltd. 1990; Andriashek et al. 1993). During the course of these investigations, 50 auger boreholes, 15 rotary boreholes, and 2 pumping wells were completed at the site. The bedrock underlying the Aurum site is the Horseshoe Canyon Formation (Andriashek et al. 1993). The bedrock mostly consists of soft, grey and greenish grey, fine-grained, bentonitic and feldspathic sandstones; grey, brown and green, silty bentonitic shales; carbonaceous shales; and coal seams. Most bedrock layers contain some or a large amount of bentonite (Irish 1970). Two bedrock channels of preglacial sand and gravel were identified. The east channel trends north-south along the eastern edge of the study area and the south

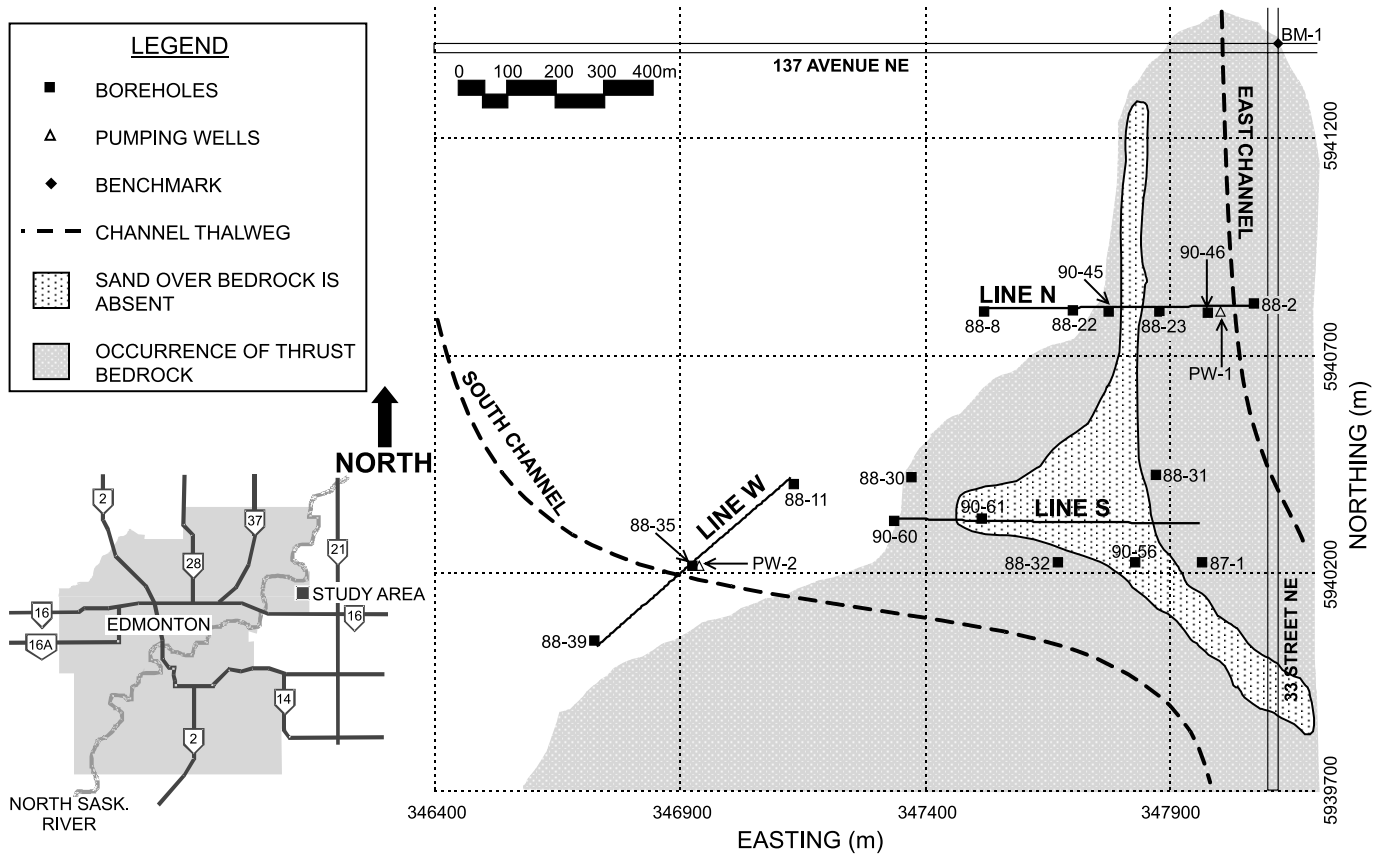
Received 23 July 2002. Accepted 28 December 2002.  
Published on the NRC Research Press Web site at  
<http://cgj.nrc.ca> on 7 May 2003.

**L.N. Meads and L.R. Bentley.**<sup>1</sup> University of Calgary, Geology and Geophysics, 2500 University Drive N.W., Calgary, AB T2N 1N4, Canada.

**C.A. Mendoza.** University of Alberta, Earth and Atmospheric Sciences, 1-26 Earth Sciences Building, Edmonton, AB T6G 2E3, Canada.

<sup>1</sup>Corresponding author (e-mail: [bentley@geo.ucalgary.ca](mailto:bentley@geo.ucalgary.ca)).

Fig. 1. Aurum site map with selected borehole and pumping well locations (interpreted geology adapted from Andriashek et al. 1993).



channel trends northwest–southeast through the middle of the Aurum site (Fig. 1). These channels are separated by ice-thrust bedrock and glacial till. The nature and extent of this separation proved difficult to resolve using borehole data alone; however, hydraulic testing demonstrated that the two channels are discrete and hydraulically unconnected (Andriashek et al. 1993). The final investigation found the Aurum site to be an unsuitable sanitary landfill site because of the potential for leachate migration into the North Saskatchewan River.

### Geophysical background

The purpose of our research is to determine whether electrical resistivity imaging (ERI) would have been valuable in the investigation of the Aurum site. Boreholes are a necessary and reliable source of primary data, and ERI interpretations provide secondary information. Although borehole data provides a good sample for a six-inch diameter vertical cylindrical volume, it can be a poor representation of the several square metres surrounding the borehole. Alternatively, ERI provides block averages of resistivity. Also, borehole data can be a more expensive data acquisition method when compared to an ERI survey. When the resistivity values are correlated with differing types of geologic materials, they can provide useful information for interpreting between boreholes.

Electrical resistivity is a function of porosity, saturation, resistivity of the pore fluids and the solid phase, and the material texture. Because sand, fine grained sediments, and

bedrock are expected to exhibit large contrasts in such properties, electrical resistivity should be well suited to resolving sand channels in bedrock and thrust bedrock in unconsolidated sediments. Electrical resistivity imaging has been used to map bedrock channels by Gilson et al. (2000), Ramag et al. (1998) and Chen et al. (1996).

Subsurface resistivity is measured by applying an electric current through two current electrodes and measuring the resulting voltage difference between two potential electrodes. The measurement is reported as apparent resistivity ( $\rho_a$ )

$$[1] \quad \rho_a = \frac{kV}{I}$$

where  $V$  is the measured voltage difference,  $I$  is the applied current, and  $k$  is a geometric factor based on the electrode arrangement (Ward 1990). The Wenner electrode array has one current electrode, followed by two potential electrodes, and ends with the second current electrode. The four electrodes are spaced an equal distance apart ( $a$  or  $a$ -spacing). The geometric factor ( $k$ ) for the Wenner array is  $2\pi a$ . The Wenner array was chosen for several reasons. It is a robust array in the presence of measurement noise. It is well suited to resolving horizontal structures because it is more sensitive to vertical changes in resistivity than to horizontal changes in resistivity (Ward 1990). The structures we are resolving are primarily horizontal. In practice, a line of multiple electrodes is deployed across the land surface. Electrodes are sequentially activated as either current or potential electrodes, and apparent resistivities are determined for numerous over-

lapping electrode configurations. These numerous measurements along a line yield a distribution of apparent resistivities for the subsurface. The apparent resistivities are then converted to true resistivity values using a numerical inversion that determines the best least-squares fit to the observed data with an objective function smoothing term that stabilizes the inversion (Ward 1990).

## Field program

The goal of this research is to investigate whether significant time and money could have been saved by using ERI and to investigate the impact of ERI results on the final site interpretation. In the following, we demonstrate that ERI results could have improved the interpretation and possibly reduced costs by allowing a scaled down borehole program. The three objectives of the ERI imaging were to (1) resolve the sand channels and terrace sands, (2) resolve the top of the thrust bedrock, and (3) resolve the sand channels beneath the thrust bedrock.

Data acquisition was completed over 4 days in early November 2001 using the Sting/Swift™ (Advanced Geosciences Inc., Austin, Tex.) ERI system. The system had 56 channels, with 4 cables and 14 electrodes on each cable. The data acquisition parameters are presented in Table 1.

Three ERI lines were run at the Aurum site (Fig. 1) on open tilled fields that had little vegetation. Each line was situated such that it corresponded with borehole transects. The three lines were surveyed with a Leica™ Total Station (Leica Geosystems, Heerbrug, Switzerland), using a benchmark (BM-1) at the intersection of 137 Avenue N.E. and 33 Street N.E. as a reference point. Line W was completed to determine if the south channel of sand and gravel could be resolved. Line S and line N were completed to view the top of the thrust bedrock and to determine if the geology below the thrust bedrock sheet could be imaged. An electrode spacing of 5 m was chosen for all three ERI lines because of the need to image deep enough to encounter the bottom of the channels (up to 40 m below ground surface) and the need for long ERI lines.

## Inversion

The raw field data were processed using Res2Dinv (Loke and Barker 1996). This computer program uses a least-squares inversion to convert measured apparent resistivity values to true resistivity values and plots them in cross-section. The program creates a resistivity cross-section, calculates the apparent resistivities for that cross-section, and compares the calculated apparent resistivities to the measured apparent resistivities. The iteration continues until a combined smoothness constrained objective function is minimized. Oldenburg and Li (1999) state that the depth of investigation cannot be determined by simple calculations and that it is dependent on the acquisition geometry, the conductivity structures, and data errors. However, they demonstrate through various modelling exercises that there is a loss of reliability in the inverted resistivity values at the bottom and ends of resistivity images where the resistivity values are least constrained by the data (Oldenburg and Li 1999). For line W, 97.8% of the calculated apparent resistivity val-

ues are within 4% of their corresponding measured value. For line S, 90.6% of the calculated apparent resistivity values are within 4% of their measured value. For line N, 94.9% of the calculated apparent resistivity values are within 4% of their measured value. Topography is accounted for in the inversion calculations. The final result is a resistivity cross-section that can be compared to geologic cross-sections.

There are several limitations to the inversion process. First, the program assumes two-dimensional geometry, in which the resistivity remains constant perpendicular to the ERI line. Second, the program averages resistivity values over data blocks. These blocks range from 5 m wide by 3 m tall near the ground surface to 5 m wide by 10 m tall at the base of the profile. Finally, the inversion algorithm favours images where neighbouring data blocks have similar resistivity values. This procedure may cause the final inversion results to be smoothed.

## Results

Inversion results and simplified borehole logs for each section are shown in Figs. 2, 3, and 4. A complete set of borehole logs used in this study can be found in the original hydrogeologic assessment report (Stanley Associates Engineering Ltd. 1990). Figure 2 shows the resistivity inversion results (iteration 5, 1.7% total average RMS error) for line W with boreholes 88–39, 88–35, PW-2, and 88–11. A thin layer of moderate resistivity (12–27  $\Omega$ -m) is observed along the top of the resistivity image. This correlates with the observed unconsolidated clay and till. The sand and gravel channel that runs through the cross-section corresponds with high resistivity values (27 to >89  $\Omega$ -m). The bottom layer has a low to moderate resistivity (<5 to 27  $\Omega$ -m) and corresponds to the bentonite-rich bedrock.

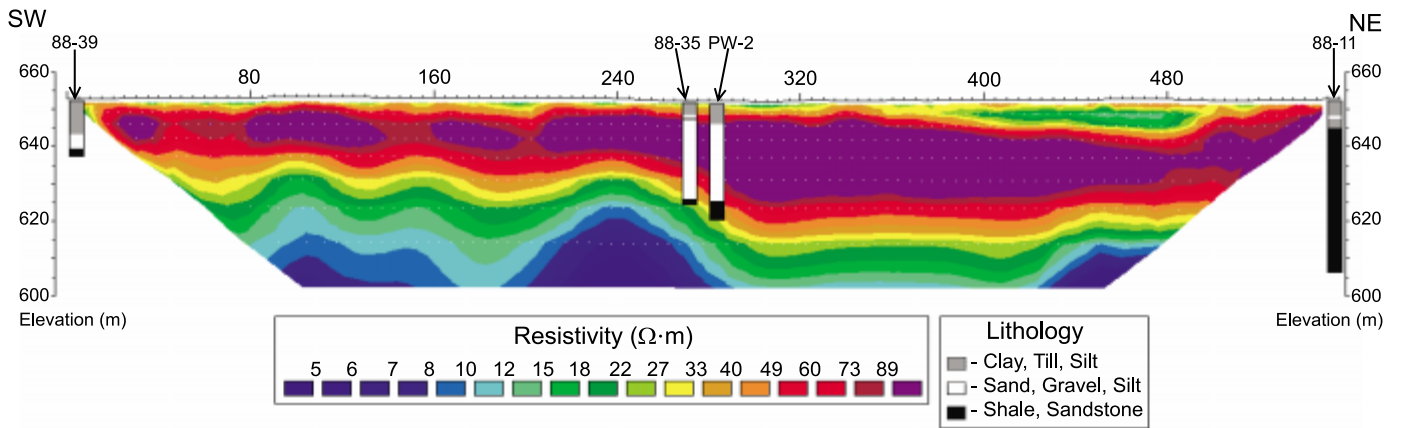
Figure 3 shows the resistivity inversion results (iteration 5, 3.4% total average RMS error) for line S with boreholes 90–60, 88–30, 90–61, 88–32, 90–56, 88–31, and 87–1. The high resistivity anomaly (49 to >89  $\Omega$ -m) at the west end corresponds well with the interpreted occurrence of terrace sand and gravel directly overlying bedrock and the absence of thrust bedrock. A low resistivity anomaly (<5 to 12  $\Omega$ -m) that correlates with the thrust bedrock in the boreholes exists near the top of the cross-section from approximately 80 m to the end of line S. Figure 1 shows that the horizontal offset from line S is 95 m for 88–31 and 80 m for 87–1, 90–56, 88–32, and 88–30. Although there are considerable offsets, there is a good correlation between the boreholes and the ERI image, especially with respect to the top of the thrust bedrock. This indicates that the top surface of the thrust bedrock is relatively uniform in this region. The two moderate resistivity layers (12–49  $\Omega$ -m) above and below the thrust bedrock correspond to the clay and till found at the Aurum site. The bottom layer in the resistivity image has low resistivity (<5 to 12  $\Omega$ -m) and is interpreted as the bedrock.

Figure 4 shows the resistivity inversion results (iteration 5, 2.3% total average RMS error) for line N with boreholes 88–8, 88–22, 90–45, 88–23, 90–46, PW-1, and 88–2. There is a high resistivity anomaly (49 to >89  $\Omega$ -m) at the west end of line N that corresponds well with the occurrence of terrace sand and gravel directly overlying bedrock and the

**Table 1.** Electrical resistivity imaging data acquisition parameters.

Location	Number of data points	Line length (m)	Minimum electrode spacing (m)	Maximum electrode spacing (m)	Maximum current (mA)	Maximum voltage (V)	Threshold noise (%)
Line S	1605	630	5	90	200	400	1
Line W	1383	560	5	90	200	400	1
Line N	1381	560	5	90	200	400	1

**Fig. 2.** Line W resistivity inversion results (borehole data from Stanley Associates Engineering Ltd. 1990). Horizontal scale in metres.



**Fig. 3.** Line S resistivity inversion results (borehole data from Stanley Associates Engineering Ltd. 1990). Horizontal scale in metres.

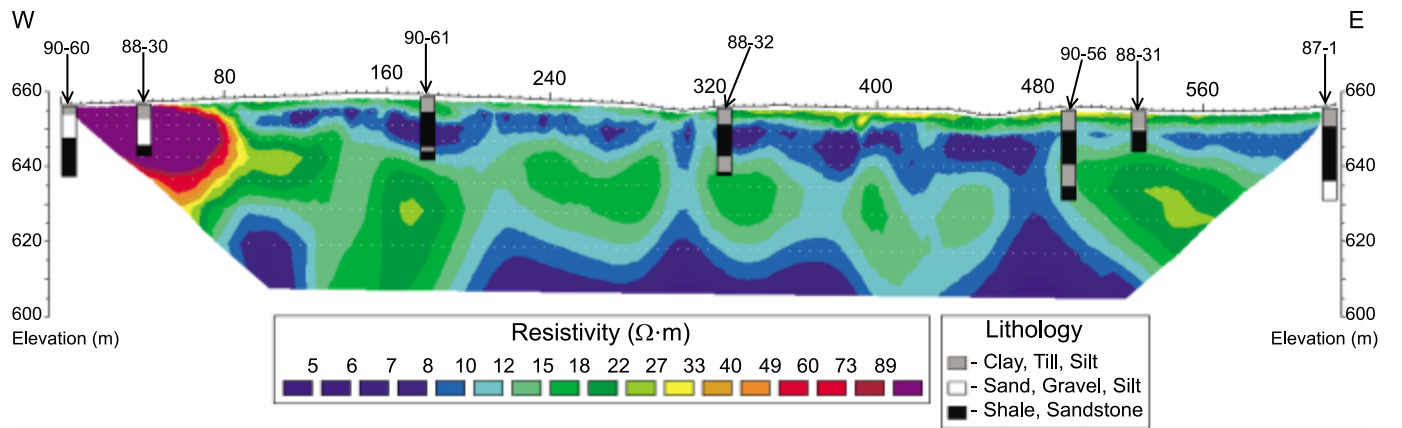
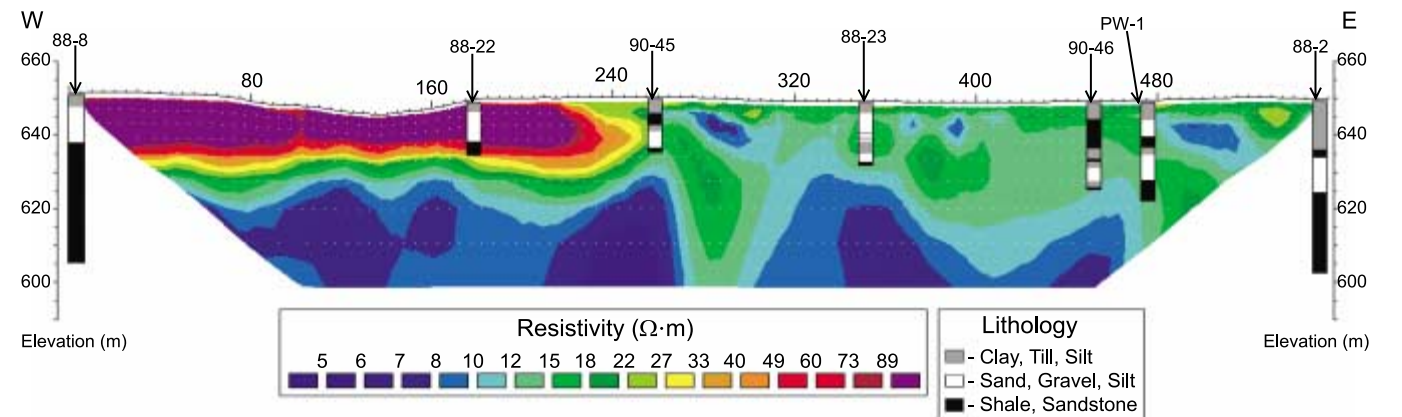


**Fig. 4.** Line N resistivity inversion results (borehole data from Stanley Associates Engineering Ltd. 1990). Horizontal scale in metres.



absence of thrust bedrock. Low resistivity anomalies (<5 to 12  $\Omega\cdot\text{m}$ ) exist near the top of the cross-section from 265 to 315 m, 365 to 375 m, 385 to 395 m, 402.5 to 412.5 m, and 475 to 525 m. These low resistivity zones are interpreted as being due to irregular blocks of low resistivity thrust bedrock. Thrust bedrock of variable thickness is also observed in the borehole logs along this section of the line. There are two moderate resistivity layers (12–49  $\Omega\cdot\text{m}$ ) above and below the thrust bedrock that correlate with the clay and till found at the Aurum site. The bedrock is the lowest layer in the resistivity image and corresponds to a low resistivity value (<5 to 12  $\text{ohm}\cdot\text{m}$ ).

A summary of the main lithologies at the proposed Aurum landfill site and the corresponding resistivity values are found in Table 2. Resistivity ranges for each line were determined by superimposing the boreholes over the ERI image and observing the correlation between the borehole lithology and the image resistivity. For each line, the sand and gravel corresponded to the highest resistivity, the bedrock and thrust bedrock corresponded to the lowest resistivity, and the clay and till corresponded to intermediate values. The low resistivity of the bedrock is due to its high bentonite content.

## Interpretation

### Terrace and channel sands

Line W was run to resolve the south channel of sand and gravel. Figure 5a shows a simplified geologic cross-section adapted from the resistivity image in Fig. 2. Figure 5b shows the geological cross-section for the same location as interpreted from the 1987–1990 investigations. The morphology of the sand channels is seen to be different, although the resistivity image matches data from the boreholes relatively well. The ERI cross-section displays a two-level channel that has a long, flat bottom and steep sides, while the 1987–1990 interpretation shows a central low and gradually sloping sides.

A portion of the terrace sands can be seen in line S and line N as a high resistivity anomaly (Figs. 6 and 7). The sands occur at the very west end of line S and the resistivity image shows the sand and gravel to be thicker than shown in boreholes 88–30 and 90–60. This poor imaging of the bottom of these sands can be attributed to a combination of reduced inversion reliability at the ends of the line, as mentioned above, inversion smoothing, and the fact that 88–30 is offset 80 m from line S. The maximum *a*-spacing for electrode arrays that were completely over the terrace sands for line S is 30% of the total maximum *a*-spacing. In contrast, the maximum *a*-spacing for electrode arrays that were completely over the terrace sands for line N is 89% of the total maximum *a*-spacing. This increased *a*-space coverage resulted in boreholes 88–22 and 88–8 on line N matching the interpreted channel thickness much better than boreholes 88–30 and 90–60 on line S. If line S had been extended further west, we expect that the inversion would have provided a better match for the depth to the bottom of the terrace sands.

The east channel runs underneath the thrust bedrock at the east end of line S and line N, and both ERI lines failed to image this channel (Figs. 6 and 7). For line S, the maximum *a*-spacing over the east channel was 17% of the total maxi-

**Table 2.** Interpreted correlation between resistivity values and site lithology.

Lithology	Resistivity values ( $\Omega\cdot\text{m}$ )	RMS error
<b>Line S</b>		3.4%
Clay and till	12 to 19	
Sand and gravel	49 to >89	
Bedrock	<5 to 12	
<b>Line W</b>		1.7%
Clay and till	12 to 27	
Sand and gravel	27 to >89	
Bedrock	<5 to 27	
<b>Line N</b>		2.3%
Clay and till	12 to 19	
Sand and gravel	49 to >89	
Bedrock	<5 to 12	

imum *a*-spacing. This degree of coverage proved to be inadequate in imaging the top of the channel sands. Line N ran directly over the east channel with a maximum *a*-spacing of 50% of the total maximum *a*-spacing, yet line N failed to resolve the sand and gravel in the channel. The failure to image the east channel is likely due to a combination of the channel being close to the end of the line, the depth of the sands, and the thinness of the beds. It may be possible that the channel sands could be imaged with a smaller electrode spacing, where there would be better resolution, or with a line centrally located over the east channel. This issue remains unresolved because logistical constraints prevent such additional surveys.

### Thrust bedrock

Figure 6a shows a simplified geologic cross-section adapted from the resistivity image of line S in Fig. 3. Figure 6b shows the geological cross-section for the same area interpreted from the 1987–1990 investigations. Figure 6a shows that the thrust bedrock has a minimum thickness of 3 m (at 520 m) and a maximum thickness of 25 m (at 420 m). Figure 6b shows that the thrust bedrock has a minimum thickness of 1.3 m (at 90 m) and a maximum thickness of 15 m (at 620 m). Although the resistivity image matches the borehole logs fairly well at their particular locations, there is a major difference in the shape of the thrust bedrock. The original interpretation depicts the thrust bedrock as a fairly uniform sheet. Our interpretation of the resistivity image indicates highly irregular, massive blocks of displaced bedrock embedded in till. Thus, it may be that bedrock was thrust in blocks by the glacial ice, instead of as a uniform sheet. A similar pattern in the interpreted thrust bedrock geometry is observed in Fig. 7. Figure 7a shows that the thrust bedrock has a minimum thickness of 2 m (at 265 m) and a maximum thickness of 14 m (at 515 m). Figure 7b shows that the thrust bedrock has a minimum thickness of 1.3 m (at 350 m) and a maximum thickness of 12.5 m (at 450 m). The broken up nature of the thrust bedrock is more pronounced in this ERI cross-section, which is in contrast with the interpreted cross-section from the 1987–1990 investigations.

The Edmonton area is characterized as a valley glaciotectonic setting, which features ice-pushed structures along the walls of the preglacial valleys (Tsui et al. 1989).

**Fig. 5.** Geologic cross-sections for line W from (a) the November 2001 ERI survey and (b) the 1987–1990 studies (adapted from Stanley Associates Engineering Ltd. 1990). Horizontal scale in metres.

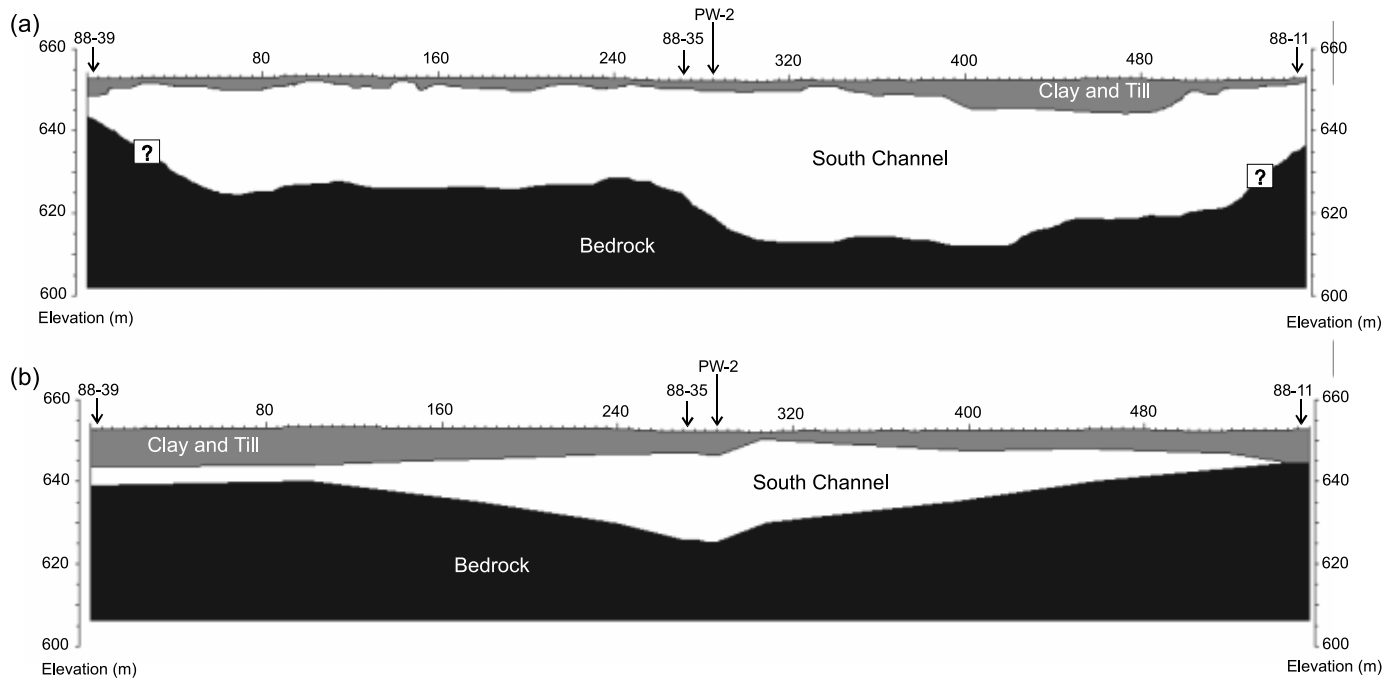
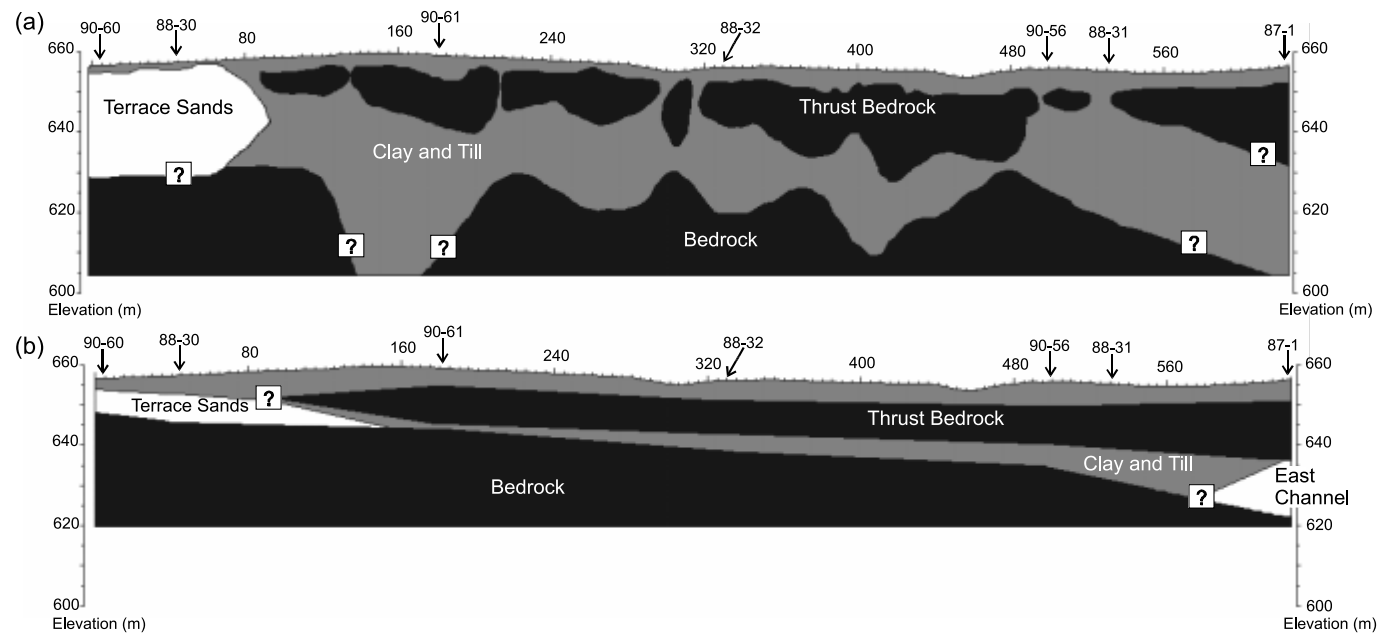


**Fig. 6.** Geologic cross-sections for line S from (a) the November 2001 ERI survey and (b) the 1987–1990 studies (adapted from Andriashek et al. 1993). Horizontal scale in metres.

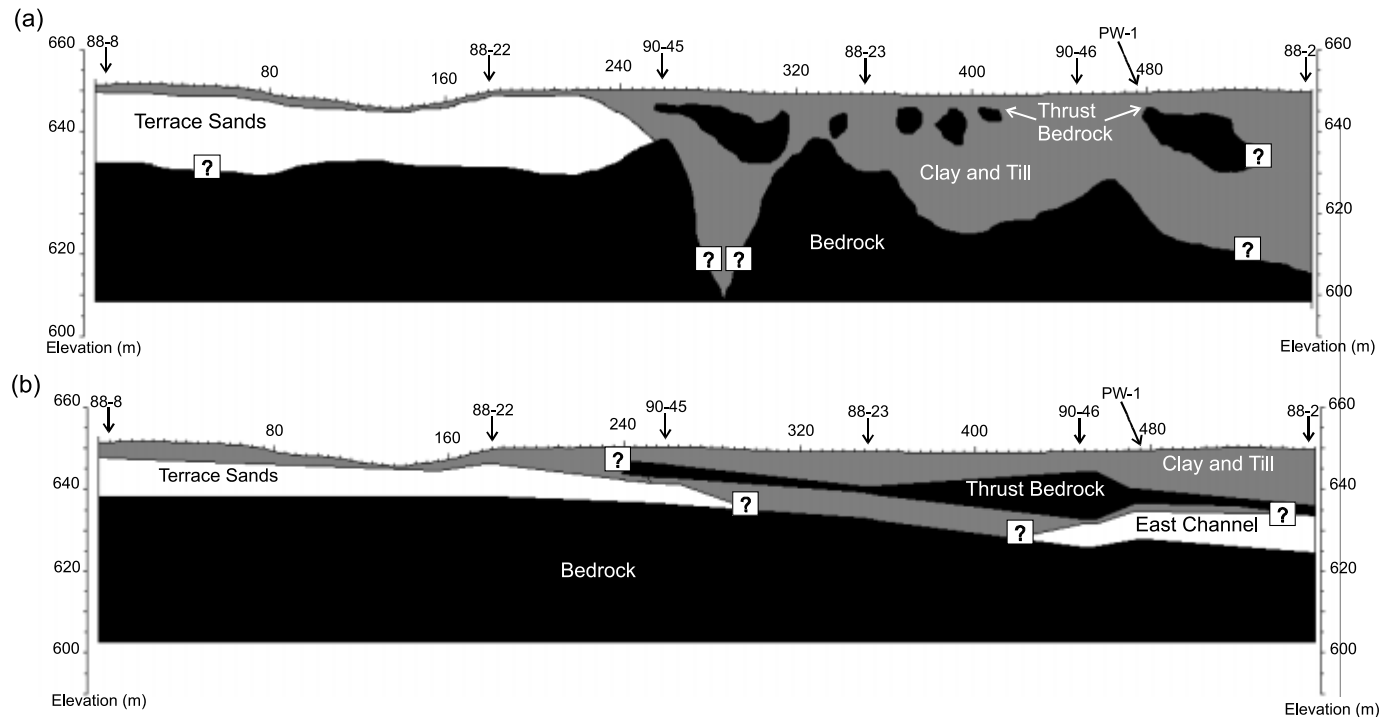


These structures are often composite ridges that consist of multiple slabs of up-thrust and contorted bedrock that may be transported (Benn and Evans 1998). It is common for the slabs to ultimately be overridden by the glacier (Bennett and Glasser 1996). The formation of composite ridges has been associated with surging glaciers (Moore 1990; Bennett and Glasser 1996; Boulton et al. 1996; and Benn and Evans 1998). The tendency of a glacier to surge is dependent on increased basal water pressures resulting from trapped

subglacial water (Benn and Evans 1998). Glaciers in the Edmonton area exhibited proglacial water ponding and increased pore-water pressures (Tsui et al. 1989). Thus, it is likely that the thrust bedrock at the Aurum site is a series of composite ridges formed by surging glaciers. Most of the resulting topographic relief was eliminated by subsequent glacial erosion.

The resistivity images are generally consistent with the borehole logs; however, there are two main inconsistencies.

**Fig. 7.** Geologic cross-sections for line N from (a) the November 2001 ERI survey and (b) the 1987–1990 studies (adapted from Andriashek et al. 1993). Horizontal scale in metres.



First, borehole 90–46 shows a large section of thrust bedrock (8.1 m thick) while the resistivity image in Fig. 4 shows no thrust bedrock. At this point we do not have an explanation for this variation. Second, the resistivity image in Fig. 4 shows no thrust bedrock at 205 m while the 1987–1990 interpretation shows 4.3 m of thrust bedrock at this point. However, the borehole log of 88–23 shows highly plastic clay interlayered with grey sand and makes no mention of thrust bedrock.

The original geologic interpretation of massive thrust bedrock sheets appears to be overly simplified. Based on the good correlation of the resistivity images to the borehole logs and the high quality of the resistivity image, the thrust bedrock appears to consist of large irregular blocks, ranging in thickness from less than 2 m to greater than 20 m, embedded in a till matrix. Consequently, the low permeability clay and till must provide the hydraulic barrier separating the east channel from the remainder of the site, rather than the thrust bedrock.

### Bedrock

The bedrock surface illustrated in Fig. 6a is very different from the bedrock surface in Fig. 6b in the region where thrust bedrock is present. The 1987–1990 investigations show a uniform bedrock surface at 13.7 m (at 80 m) to 20.3 m (at 495 m) depth. The ERI cross-section shows a variable bedrock surface as shallow as 24 m below ground surface (at 305 and 480 m). The resistivity image indicates that the bedrock surface is as deep as 40 m below ground surface (at 125–190 m). However, as discussed previously, the inversion resistivity values at the bottom of the profile are poorly constrained, and the resulting interpretation is un-

certain. The bedrock surface shown in Fig. 7a is similar to that observed in Fig. 6a. The interpretation from the 1987–1990 investigations shows the bedrock as uniform; however, the resistivity image shows a variable bedrock surface (from 10 m to possibly greater than 40 m below ground surface). The occurrence of bedrock in boreholes 90–46 (Fig. 3) and 90–45, 88–23, 90–46 and PW1 (Fig. 4) correlate with the bedrock surface in the ERI cross-section; however, there is a tendency for the ERI images to overestimate the depth to bedrock. This is due to two imaging problems. First, the data blocks range from 3 to 10 m, resulting in a maximum resolution of 1.5–5 m. Therefore, it is not possible to locate any features more accurately than to within 1.5–5 m. Second, as discussed above, the inversion algorithm tends to smooth the ERI image. This causes sharp contrasts in resistivity to appear as though they are gradational contacts. Given that the ERI cross-sections match the physical borehole data, we interpret the bedrock surface to be an irregular surface.

Figures 6 and 7 depict the bedrock surface under the terrace sands as a more uniform surface. This is an area where the bedrock has not been modified by glacial ice. The morphology of the bedrock surface in this area is the same in both the resistivity interpretations (Fig. 6a and 7a) and the borehole interpretations (Figs. 6b and 7b). Again, the resistivity image in Fig. 3 shows a deeper bedrock surface because of the imaging limitations discussed above.

The resistivity images indicate a much more irregular bedrock surface outside of the terrace sands. This is consistent with bedrock being modified by glacial ice and having portions of it removed and transported as thrust bedrock. The morphology of the bedrock surface in the resistivity image is consistent with the interpretation that the surface is uneven

where glacial activity has altered it and that the surface is a typical erosional surface where the glaciers have not had an effect.

## Conclusions

The goal of this study was to investigate whether ERI could be used to come to the same conclusions as the previous studies in 1987–1990. We found that the ERI survey at the Aurum site allowed an expansion on the conclusions that were previously reached. The ERI was easily able to resolve the south channel in surrounding bedrock and delineate the top of the thrust bedrock surface, but was unable to resolve the east channel beneath the thrust bedrock. In addition, the ERI survey was able to resolve the bedrock surface underneath the thrust bedrock. A combined interpretation using the ERI survey and available borehole logs was able to provide a more detailed picture of the Aurum site. The bedrock surface is highly variable and ranges from less than 10 m below ground surface to possibly more than 40 m below ground surface. The bedrock surface underneath the terrace sands is a flat erosional surface. The thrust bedrock occurs as erratic massive blocks that are less than 2 m to greater than 30 m thick. The south channel has a long and flat bottom, two levels, and abruptly sloping sides.

We estimate that the commercial cost of this ERI survey would be \$10 000 to \$15 000CAN. The cost of drilling a 15 m deep auger borehole is \$1000 to \$1500CAN. Our results show that, even at such a large scale, the borehole data by itself was still too sparse to capture the details of the complex geology at the proposed Aurum landfill site. The 1987–1990 studies completed 50 auger boreholes, 15 rotary boreholes and two pumping wells at the site. By replacing 10–15 auger boreholes with a 3 line ERI survey, an integrated program that included 35–40 auger boreholes, 15 mud rotary boreholes, 2 pumping wells, and 3 ERI lines could be completed for the same cost as the 1987–1990 investigations. As well, if ERI surveys were completed prior to drilling, the results would help locate strategic boreholes. Thus, an integrated geophysical, geologic, and hydrogeologic study would have provided a more rapid and accurate understanding of the geology at the Aurum site.

## Acknowledgements

The authors would like to thank the Natural Sciences and Engineering Research Council (NSERC) for their support to make this research possible. We also give thanks to Laurence Andriashek at the Alberta Research Council and Mehran Gharibi at the University of Calgary for their information and assistance with the field research.

Brian Smerdon and Arif Alkalali at the University of Alberta assisted with the fieldwork. Access to the site was kindly granted by Jack Agrios, QC, on behalf of the landowner and the lessee, André Moizard.

## References

- Andriashek, L.D., Thomson, D.G., and Jackson, R. 1993. Edmonton landfill site investigation: a case study applying hydraulic information to interpret a glacially disturbed site. *Geoscience Canada*, **20**(4): 157–164.
- Benn, D.I., and Evans, D.J.A. 1998. *Glaciers and glaciation*. Arnold, London.
- Bennett, M.R., and Glasser, N.F. 1996. *Glacial geology; ice sheets and landforms*. John Wiley & Sons, Inc., Chichester.
- Boulton, G.S., van der Meer, J.J.M., Hart, J., Beets, D., Ruegg, G.H.J., van der Wateren, F.M., and Jarvis, J. 1996. Till and moraine emplacement in a deforming bed surge — an example from a marine environment. *Quaternary Science Review*, **15**: 961–987.
- Chen, W., Xuanqing, Z., Naihua, H., and Yonghong, M. 1996. Compiling the map of shallow-buried palaeochannels on the North China Plain. *Geomorphology*, **18**(1): 47–52.
- Gilson, E.W., Nimeck G., Bauman P.D., and Kellett, R. 2000. Groundwater exploration in prairie environments. *In Proceedings of the Symposium on the Application of Geophysics to Engineering and Environmental Problems*. Arlington, Va., 20–24 February. *Edited by* M.H. Power, A.B. Ibrahim, and L. Cramer. Environmental and Engineering Geophysical Society, Wheat Ridge, Colo., pp. 955–959.
- Irish, E.J.W. 1970. The Edmonton group of south-central Alberta. *Bulletin of Canadian Petroleum Geology*, **18**(2): 125–155.
- Loke, M.H., and Barker, R.D. 1996. Rapid least-squares inversion of apparent resistivity pseudosections by a quasi-Newton method. *Geophysical Prospecting*, **44**: 131–152.
- Moers, H.D. 1990. Ice-marginal thrusting of drift and bedrock: thermal regime, subglacial aquifers, and glacial surges. *Canadian Journal of Earth Sciences*, **27**: 849–862.
- Oldenburg, D.W., and Li, Y. 1999. Estimating depth of investigation in DC resistivity and IP surveys. *Geophysics*, **64**(2): 403–416.
- Ramag, J.M., Gardner, T.W., and Sasowsky, I.D. 1998. Early Pleistocene glacial Lake Lesley, west branch Susquehanna River Valley, central Pennsylvania. *Geomorphology*, **22**(1): 19–37.
- Stanley Associates Engineering Ltd. 1990. Hydrogeologic assessment — Edmonton Waste Management Centre. Report 48–115–01–01. Edmonton, Alta.
- Tsui, P.C., Cruden, D.M., and Thomson, S. 1989. Ice-thrust terrains and glaciotectionic settings in central Alberta. *Canadian Journal of Earth Sciences*, **26**: 1308–1318.
- Ward, S.H. 1990. Resistivity and induced polarization methods. *In Geotechnical and environmental geophysics*. *Edited by* S.H. Ward. Society of Exploration Geophysicists, Tulsa, Okla., Vol. 1, pp. 147–189.